# A PROPOSAL FOR THERMAL COMPUTATIONAL MODEL FOR API 5L-X80 STEEL FRICTION STIR WELDS BASED ON THERMOCOUPLES MEASUREMENTS

G. G. DE SOUSA*, M. MONTOYA*, N. BOUCHONNEAU*, T. F. C. HERMENEGILDO* and T. F. A. SANTOS*

**Universidade Federal de Pernambuco, Av. da Arquitetura, s/n, Post Code: 50740-550, Recife, Brazil, https://orcid.org/0000-0003-2273-0760, * tiago.felipe@ufpe.br*

*DOI 10.3217/978-3-85125-615-4-33*

ABSTRACT

This work aims to validate a computational model suitable for predicting temperature distribution of API 5L-X80 steel welded joints manufactured by Friction Stir Welding. The model was verified through comparative analysis between experimental data and a computational model generated from a commercial finite element method software. The testing data was acquired by temperature measurements, using thermocouples positioned equally spaced along a workpiece plate of 12 mm thick during the welding process. The experiment was conducted with two different sets of heat inputs and rotational pin speeds: a joint with heat input of 1.69 KJ.mm$^{-1}$ and 300 rpm (cold joint), and the other with a heat input of 1.91 KJ.mm$^{-1}$ and 500 rpm (hot joint). Temperature data was processed and used to preview the material's thermal cycle. The computational model was developed using the COMSOL Multiphysics® software, as the heat source was considered stationary in a Eulerian model. The model was calibrated for both joints and comparison between measured temperatures with thermocouples results have showed significant similarities when the maximum simulated thermal cycles and the experimental temperature data are compared. The thermal model was also used to predict maximum temperatures the thermal history for points of the welded region where is physically impossible to perform experimental temperature measurements due to the presence of the pin and the tool's shoulder.

Keywords: Friction Stir Welding, Computational Modelling, API 5L-X80 Steel Joints

## INTRODUCTION

Friction stir welding (FSW) is a solid-state welding and joining process, developed and patented by The Welding Institute (TWI) in 1991 [1]. This manufacturing process has been successfully conducted in aluminum, titanium, copper, zinc and lead alloys. Advantages in employing FSW, among others, are: joints with superior mechanical properties due to dynamic re-crystallization and minor distortions in the workpiece [2], leading to a less damaging manufacturing process and stable union of the joint; an environmentally harmless

process, producing few machining waste and requiring minimum or no surface cleaning. Recently, the attention of shipbuilding industries and petrochemical producers was drawn towards the feasibility of friction stir welding high temperature alloys such as steels stainless steels and High Strength Low Alloy (HRLA) steels [3-5]. HRLA steels such as the API 5L-X80 are more suitable to pipeline and offshore construction owing to a combination of suitable microstructure and strength, making this type of material more adequate for oil and gas pipelines [6,7]. These steels are characterized by low carbon content, which results in higher tenacity in the HAZ after welding processes, and by the presence of alloying elements, such as Nb, V, Ti, Cr, Mo, Ni and B [8].

The API 5L-X80 used in this study has a carbon equivalent (C.E) of 0,17 following the API 1104 standard [9]. This provides a good weldability index for this material and the possibility of application in a future industrial production line using FSW. The increasing necessity for a FSW computational model, in order to provide an understanding of the thermal phenomena of X80 welding joints manufactured by this process, was the driving force for this work. The adequate microstructure, which allows high structural commitment depends on welding thermal cycles whichever the process, but specially friction stir welding that combines high degree of deformation and elevated temperature. Due to this fact, this work focuses on validating a computational thermal model proposed to preview temperature distribution and thermal cycles in the advancing side of API 5L-X80 steel welds manufactured by FSW. Computational pure thermal models are some of the accessible approach to predict thermal cycles in FSW. They provide a practical and straightforward perception of the heat distribution along the welding line [10]. In this work, the advancing side was chosen owing to be a major concern regarding the nugget integrity, where a zone of high hardness tends to appear at high cooling rates [11].

**Table 1** The API 5L-X80 steel chemical composition used in this study (wt%)

| C | Nb | Al | Mn | V | Si | B | Cu |
|---|---|---|---|---|---|---|---|
| 0,05 | 0,066 | 0,035 | 1,76 | 0,025 | 0,17 | 0,03 | 0,02 |
| **P** | **S** | **Cr** | **Ni** | **Ti** | **N** | **Ca** | **Mo** |
| 0,016 | 0,002 | 0,15 | 0,02 | 0,016 | 0,0059 | 0,003 | 0,20 |

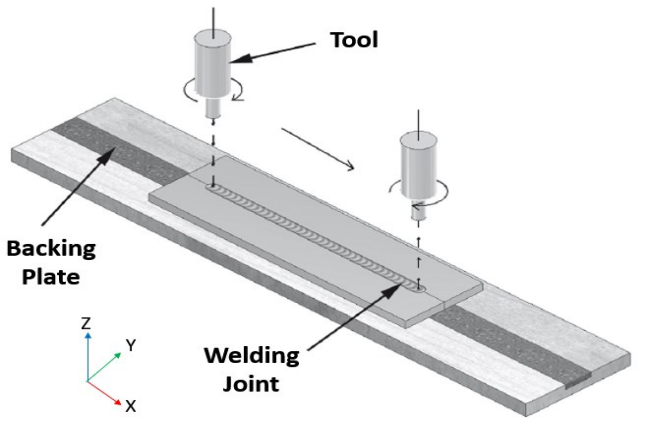

**Fig. 1** Schematics of the FSW process showing the tool´s shoulder moving along the joint, adapted from Santos *et al*. [12].

## EXPERIMENTAL PROCEDURE

### WELDING AND THERMAL HISTORY ACQUISITION

The welded joints were produced from two X80 plates of 110 × 400 × 12 mm, which were placed in a ceramic backing plate and butt welded along their largest dimension, resulting in weld of 380 mm in length, as illustrated in Fig. 1. Due to the dimensional limitations of the PCBN pin's length (5.7 mm) ceramic tool used, the joints were manufactured by two welding passes, one on each side of the plate. After the welding procedure, the PCBN tool's structural integrity was visually verified, neither wear nor broken fragments were found on the pin and shoulder surface. To measure the thermal history at specific locations, an experimental setup was developed with eight K type thermocouples attached to both sides of the joint, positioned at 2 mm below the surface of the plate. During the welding procedure temperature measurements were carried out with these thermocouples positioned along the workpiece, at distances of 6, 8, 10 and 12 mm from the welding line. Fig. 2 has the detailed arrangement of the thermocouples used during the welding procedure. Although there are minor reports regarding the estimation of energy imposed in the FSW process, the heat input was calculated by the following equation:

$$HI = \left( \frac{\omega \cdot M}{1000 \cdot u_{welding}} \right) \cdot \eta \tag{1}$$

The welding procedure was conducted with a set of parameters leading to a lower heat input of 1.69 kJ.mm$^{-1}$ (cold joint), and a greater heat input of 1.91 kJ.mm$^{-1}$ (hot joint). Values of tool's translational speed ($u$), rotational speed ($\omega$) and the input torque ($M$) were calculated and acquired by experimental data and are shown in Table 2. The acquisition data from the input parameters used in the FSW process was recorded and analyzed to measure maximum temperatures and to generate thermal cycles for each joint.

**Table 2** FSW Experimental parameters – Hot Joint and Cold Joint

| Weld Joint | Heat Input [kJ.mm$^{-1}$] | $u$ - Welding Speed [m.s$^{-1}$] | $\omega$ - Rotational Speed [rpm] | $F$ - Axial Force [kN] |
|---|---|---|---|---|
| Hot | 1.91 | 1.67 | 500 | 35.8 |
| Cold | 1.69 | 2.00 | 300 | 29.8 |

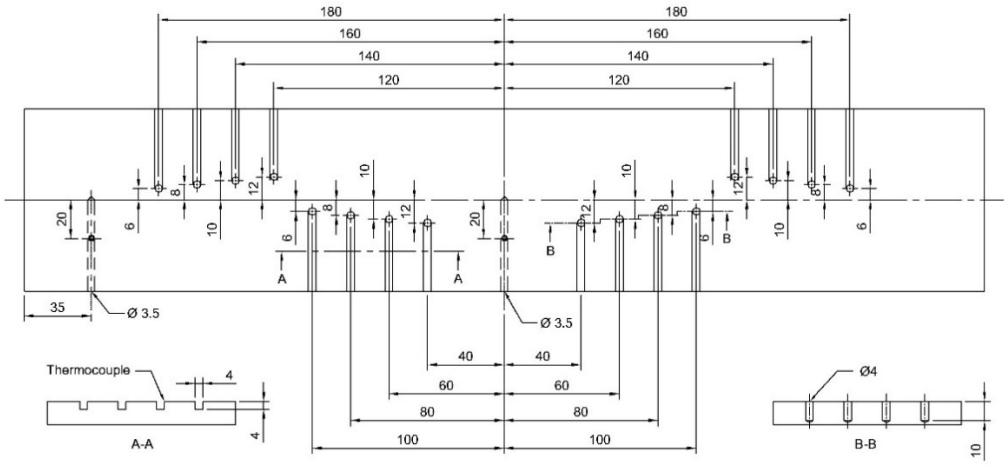


**Fig. 2** Thermocouple arrangement used during the FSW experimental setup.

## COMPUTATIONAL THERMAL MODELLING

A computational thermal model was developed using the COMSOL Multiphysics® heat transfer module. Being previously calibrated, the model is proposed to preview temperature distribution and thermal history in the advancing side of the welds at positions/distances from the welding line where is physically/extremely difficult to conduct temperature measurements by thermocouples due to the presence of the pin and shoulder. In order to reduce the processing time of the computational calculations the model geometry is considered to be symmetric along the welding line, and thus half of the joint was modelled and enmeshed. More details can be found in Fig. 3.

The following equation defines the heat transfer in the plate, with the above assumption:

$$\nabla\left(-k\cdot\nabla T\right)=Q-\rho\cdot C_{p}\cdot u\cdot\nabla T \tag{2}$$

The stationary heat source, with a 90% efficiency ($\eta$ = 0.90) [13], was modelled based on previous works of Song and Kovacevic [14] and Schmidt and Hattel [10], in which a flat shoulder, with no tilt angle, contributes to a surface heat flux (purely frictional) and the pin shares a volumetric heat contribution. The tool was modelled having a conical pin with the following dimensions: $R_p$ = 5 mm, $R_{tip}$ = 1.8 mm $H_p$ = 5.7 mm being the pin's radius, the pin's tip radius and the pin´s height. The pin's heat contribution is considered to be:

$$Q_{pin}=\left(\frac{f_{pin}\cdot M\cdot\omega}{V_{pin}}\right)\cdot\eta \tag{3}$$

In the pin's equation the $f_{pin}$ is the factor related to the percentage heat generation from the pin and estimated to be ≈ 20% according to Colegrove [15], $\omega$ is the tool's rotational speed (rev min$^{-1}$), and $M$ is the average torque measured in welding (Nm s$^{-1}$).

The shoulder geometry was modelled as: $R_{shoulder}$ = 12.0 mm and $H_{shoulder}$ = 5.7 mm. The total heat expression at the shoulder/workpiece interface can be defined by:

$$Q_{shoulder} = \omega \cdot r\left[(1-\delta)\mu \cdot \tau_{friction} + \delta \cdot \tau_{yield}\right] \cdot \eta \tag{4}$$

In this equation: $r$ is the radial distance from the tool's center axis to the tool's shoulder, $\mu$ is friction coefficient, $\tau_{friction}$ is the forging pressure related to the applied normal force, and $\delta$ is the contact variable which balances the heat generated by plastic deformation ($\tau_{yield}$) and by friction ($\tau_{friction}$). In this work we assume the contact condition ($\tau_{contact}$) being independent of temperature, strain rate and also being in equilibrium with the pressure distribution ($\tau_{friction}$), leading to a value of $\delta = 0$. This previous assumption leads to a sliding condition:

$$Q_{shoulder} = \left(1 - f_{pin}\right) \cdot \omega \cdot r \cdot \mu \cdot \tau_{friction}, \quad \tau_{friction} = \frac{F_N}{A_S} \tag{5}$$

In which $F_N$ is the forging pressure, and $A_s$ is the shoulder's surface area. The friction coefficient is considered to be variable during the welding, to simplify a value of $\mu$ = 0,4 was chosen as used by [14]

The FSW is, innately, a solid-state manufacturing process, with the workpiece reaching 70 - 90% its melting point or solidus temperature [15, 16]. To transport this fact to the current model a calibration was done by comparing simulated temperatures with temperatures registered by the thermocouple at 8 mm from the welding line. At this distance one can assume/infer/presume there was no interference from the tool in measured temperatures by the thermocouple. A step condition was inserted limiting the maximum temperature reached by the model, as made by [14] setting the heat flux to zero when the temperature reaches values greater than $T_{solidus}$ of the workpiece [17].

$$Q_{shoulder}(r,T) = \begin{cases} Q_{shoulder}, if \;\; T < T_{\text{solidus}} \\ 0, if \; T \geq T_{solidus} \end{cases} \tag{6}$$

At such high temperatures, radiation cannot be neglected and it is brought to the model with insertion of an emissivity coefficient $\varepsilon$ = 0,3 applied all over the workpiece surface and the tool.

$$q_{totalloss} = \sigma \cdot \varepsilon\left(T^4_{env} - T^4\right) + h \cdot \left(T_{env} - T\right) \tag{7}$$

The heat losses in the model were defined as general outflux and where applied all over the upside and the downside of the workpiece. In the above equation. $\varepsilon$ is the surface emissivity of the tool and the workpiece, $\sigma$ is the Stefan-Boltzmann constant, $T_{env}$ is the environment temperature and $h$ refer to the convective coefficients associated with the surfaces present in the model (surface of the workpiece and the exposed area of the tool).

The convective coefficients at the upper surface and at the downside of the workpiece were estimated to be $h_{upside}$ = 10 W m$^{-2}$K$^{-1}$ e $h_{downside}$ = 100 W m$^{-2}$K$^{-1}$. The backing plate has its conductive coefficient lumped into a general convective coefficient with different values, $h_{backing\text{-}cold}$ = 600 W m$^{-2}$K$^{-1}$ for the cold joint and $h_{backing\text{-}hot}$ = 200 W m$^{-2}$K$^{-1}$ for the hot joint. [18,19]. These values were considered once taking the forging pressure $F_N$ related influence on the gap conductance between the workpiece and the backing plate [14,18,19]. As for the tool, values of a lateral and top coefficients were considered $h_{shoulder\text{-}lateral}$ = 15 W m$^{-2}$K$^{-1}$ and $h_{shoulder\text{-}top}$ = 20 W m$^{-2}$K$^{-1}$, respectively regarding convective and conductive heat losses due to high temperature values achieved by the tool material.

**Table 3** API 5L-X80 thermophysical properties. Adapted from Rocha *et al* [20].

| Temperature [ºC] | Thermal Conductivity [W m$^{-1}$ ºC$^{-1}$] | Specific Heat [J kg$^{-1}$ ºC$^{-1}$] |
|---|---|---|
| 0 | 51.062 | 571.235 |
| 100 | 510.62 | 571.235 |
| 200 | 47.324 | 571.235 |
| 300 | 43.840 | 571.235 |
| 400 | 40.424 | 614.841 |
| 500 | 29.634 | 686.617 |
| 550 | 33.546 | 730.831 |
| 600 | 26.461 | 780.774 |
| 650 | 18.019 | 868.623 |
| 700 | 14.874 | 977.691 |
| 750 | 11.386 | 841.431 |
| 800 | 14.735 | 790.265 |
| 900 | 14.735 | 608.333 |
| 1200 | 14.735 | 681.529 |

The steel's density was considered to be constant, with a value of ρ = 7860 kg m-3. The alloy´s thermophysical properties were implemented in the workpiece according to data provided by the work of Rocha et al [20] and shown in the Table 3.

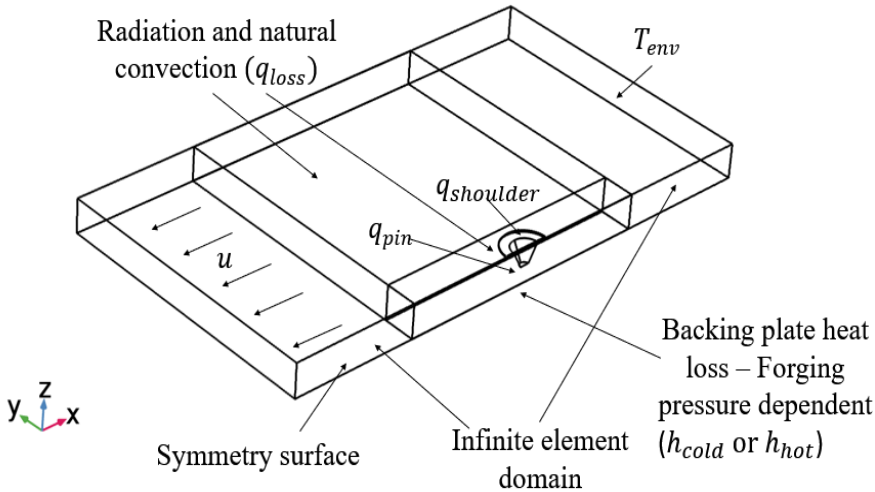


**Fig. 3** The model geometry with a reduced size illustrating zones and considerations.

The material used for the tool, Polycrystalline Boron Cubic Nitride (PCBN), had to be implemented as a new material in the program library with the data from Table 4. This material must withstand high temperatures and be chemically inert. The final enmeshed geometry was composed of 25125 tetrahedral elements and 52274 DOFs detailed in Fig. 4.

**Table 4** PCBN termophysical properties [13]

| Density [Kg.m$^{-3}$] | Thermal Conductivity [W m$^{-1}$ ºC$^{-1}$] | Specific Heat [J kg$^{-1}$ ºC$^{-1}$] |
|---|---|---|
| 3120 | 130 | 1966 |

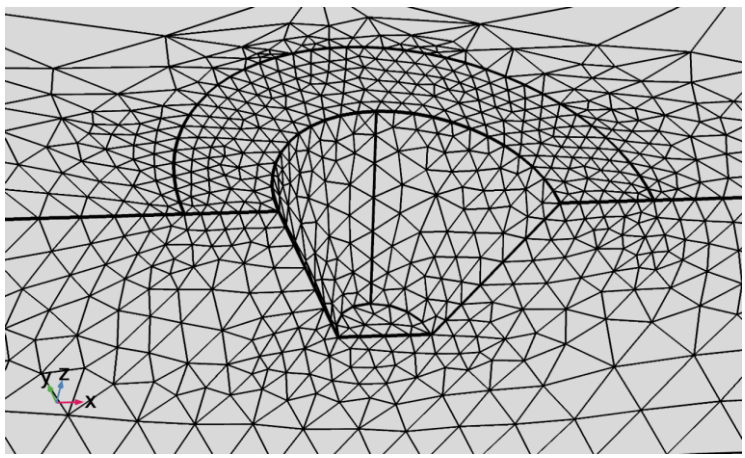


**Fig. 4** Detailed meshed geometry of the tool and the workpiece with tetrahedral mesh elements.

## RESULTS AND DISCUSSION

The model was verified and validated through comparative analysis between experimental data and simulated results for both joints. The maximum temperature values estimated by the model at the closest thermocouple was 992 ºC for the hot joint and 873 ºC for the cold joint. The simulated curves had a considerable agreement with the experimental values for maximum values as well as cooling rates.

**Table 5** Comparison between the simulated and experimental temperatures for the advancing side of welds, at different distances from the welding line – Hot Joint and Cold Joint.

| Weld Joint | 6 mm | 8 mm | 10 mm | 12 mm |
|---|---|---|---|---|
| Hot | 989 ºC | 913 ºC | 815 ºC | 567 ºC |
| Hot-Simulated | 992 ºC | 915 ºC | 805 ºC | 676 ºC |
| Cold | 880 ºC | 794 ºC | 753 ºC | 510 ºC |
| Cold-Simulated | 873º C | 793 ºC | 673 ºC | 566 ºC |

**Table 6** Simulated temperature for neighboring distances of the welding line.

| Weld Joint | 0 mm | 2 mm | 4 mm |
|---|---|---|---|
| Hot-Simulated | 1222 ºC | 1215 ºC | 1159 ºC |
| Cold-Simulated | 1114 ºC | 1106 ºC | 1041 ºC |

The simulated and experimental maximum temperatures for the advancing side of both joints are shown in Table 5.

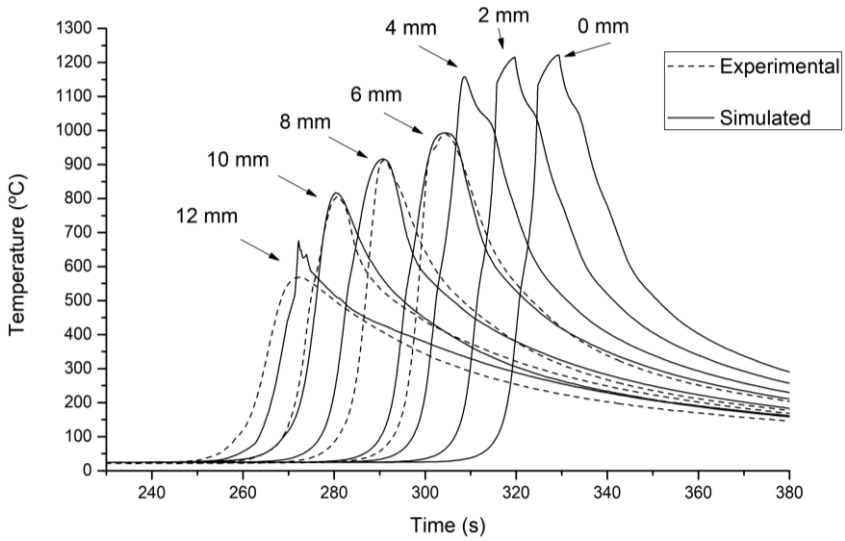


**Fig. 5** Comparative graphic showing simulated and experimental thermal cycles of FSW considering a hot joint.

For the cold joint thermal cycles represented in Fig. 7, it can be recognized from that the experimental data curve for the 6 mm thermocouple is slightly altered. As this thermocouple was next to the tool zone this shift might represent a disruption in temperature acquisition during the welding, caused by the sudden contact with the tool. This fact can be reassured by the style of the simulated temperature curve for 4 mm, 2 mm and 0 mm, in which one can notice the different shape of the slope for simulated thermal cycles in regions situated around the pin. The simulated temperatures for the cold joint in Table 5 still helps to preview what would have been the correct values for the experimental temperatures, had the tool not touched the thermocouples.

Temperatures simulated for the welding line are slightly lower for the cold joint, as shown in Fig. 7. This can be justified by a lower heat input, leading to greater cooling rates imposed during welding. An overall precise temperature prediction was achieved for both simulations. The exceptions are the thermal cycles for thermocouples situated at 12 mm from the welding line, where the maximum simulated temperatures are slightly overpredicted. The "spike-like" curve of the last simulated temperature can be justified due to temperature data acquisition from the tool´s edge, measuring temperatures coming from a transition zone (shoulder/workpiece) of the model. These differences concerning simulated and measured temperatures might also be due to simplifications of the current thermal model, which ignores the heat contribution by the material flow around the tool [21]. As proposed by Schmidt and Hattel [22], a pure thermal model is capable of predict the non-uniform thermomechanical conditions in the shear region to a certain degree. Furthermore, if one assumes an equilibrium of contact pressure and its temperature independence, one is not accounting for the plastic heat dissipation contribution. This fact has a direct influence on temperature prediction for external zones of the weld, as can be seen in the major difference for the last thermocouples in both conditions.

For simulated temperatures much closer to welding line (at 0, 2 and 4 mm), the model had a reliable agreement with both conditions, as can be noted in Table 6. As expected, simulated temperatures in this region were higher for the hottest condition than for the cold condition. The surface maximum temperature computed for both conditions can be view in Fig. 6 and Fig. 8. Both are located right behind the tool along the welding line, having a value of 1235 ºC for the hot joint and 1140 ºC for the cold joint. These values share a position similarity with the work of Santos *et al*. [21], in which maximum surface temperatures were simulated and can be found in the trailing side of the tool. In Table 6, higher values of simulated temperatures at 0 mm in both conditions are in agreement with the location, as maximum temperatures are generally measured along the welding line and are located in the proximities of the shoulder region [22]. The simulated values are also in agreement with previous works, since FSW of low carbon steel and stainless steel is likely to provide joints with extreme temperatures, ranging from 1000 ºC in the TMAZ to 1300 ºC in the SZ welding line. [23].

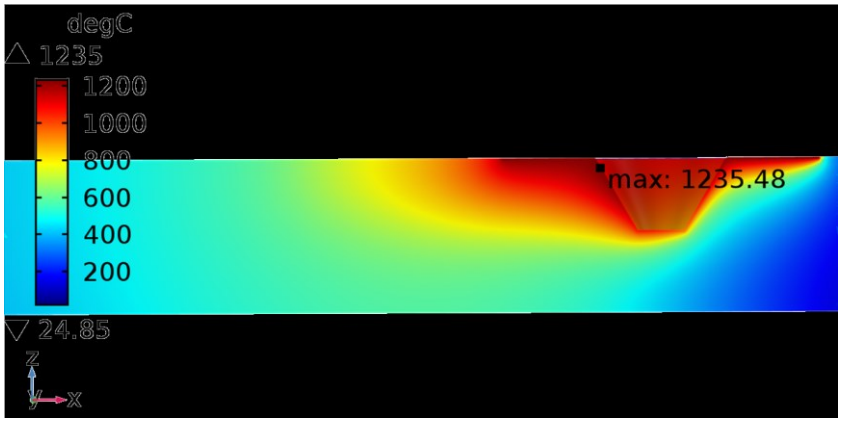


**Fig. 6** Simulation result of FSW considering a hot joint, showing the location of maximum temperature on the workpiece surface.

Multiple works [19,22,24] have credited the differences between simulated and experimental temperatures on the difficulty of finding a definite experimental convective coefficient for the workpiece/backing plate interface. Schmidt and Hattel [22] concluded that one can obtain a reasonable agreement with minor adjusts in these convective values.

The usage of a backing plate during the FSW procedure allows the X-80 welding joint to be more thermally isolated and to receive higher normal forces (forging pressures), as concluded by Santos *et al* [12]. This is also proposed in the current thermal model, as the adopted values for the convective coefficient values are distinct for best fitting with the experimental data and also are considered dependent from the forging pressure.

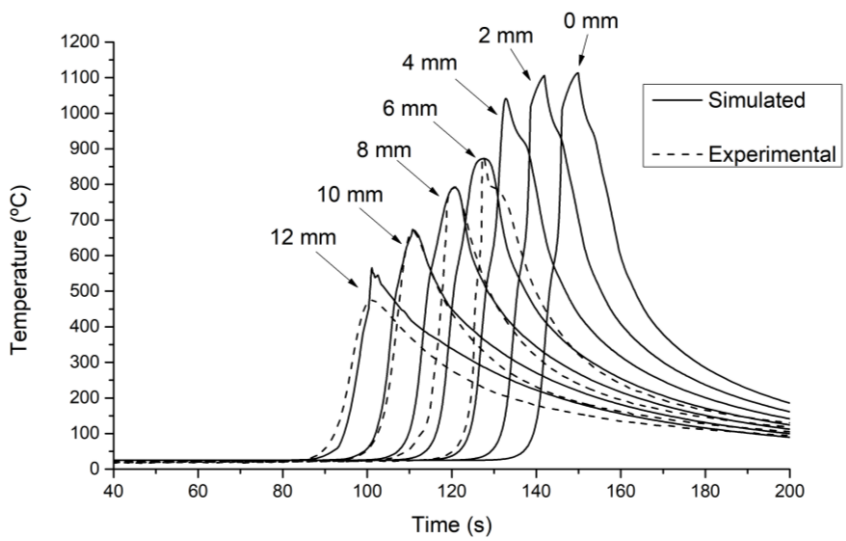


**Fig. 7** Comparative graphic showing simulated and experimental thermal cycles of FSW considering a cold joint.

This work also allows a good correlation with the work of Hermenegildo *et al.* [3], which has found a remarkable microstructure variation for the advancing sides of both welding conditions. The computational model simulated that temperatures of the workpiece around the tool's vicinity reached values higher than the $A_{r3}$ temperature ($A_{r3}$ = 735 ºC).

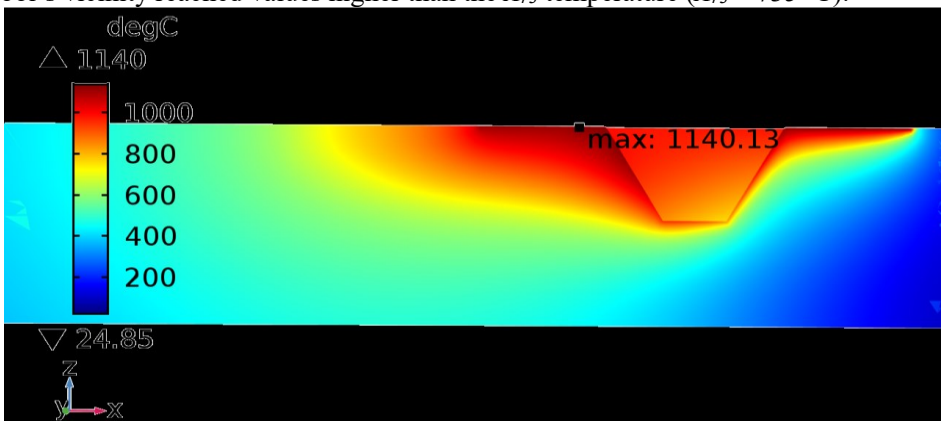


**Fig. 8** Simulation result of FSW considering a cold joint, showing the location of maximum temperature on the workpiece surface.

As proposed in Fig. 9 for the hot joint, simulated temperatures within the hard zone of the welding line (at 0, 2 and 4 mm) are superior than the recrystallization temperature ($T_{nr}$) estimated for this material by the same authors ($T_{nr}$ = 899 ºC) [3], which, coupled with a lower cooling rate (21.4 ºC.s$^{-1}$) than that of cold joint (31.0 ºC.s$^{-1}$) would lead to a growth in austenite grain around the nugget zone, and eventually, the presence of martensite in this region, at the advancing side. As previous works of Santos *et al.* [25] have shown for comparable welding conditions, in the stir zone the hot joint presented CTOD values below the minimum requirements for offshore applications (DNV-OS-101 standards), whereas for the cold joint the CTOD values were higher. This confirms the potential of this work to estimate temperatures and to analyze welding conditions which are critical for the mechanical performance of the joints.

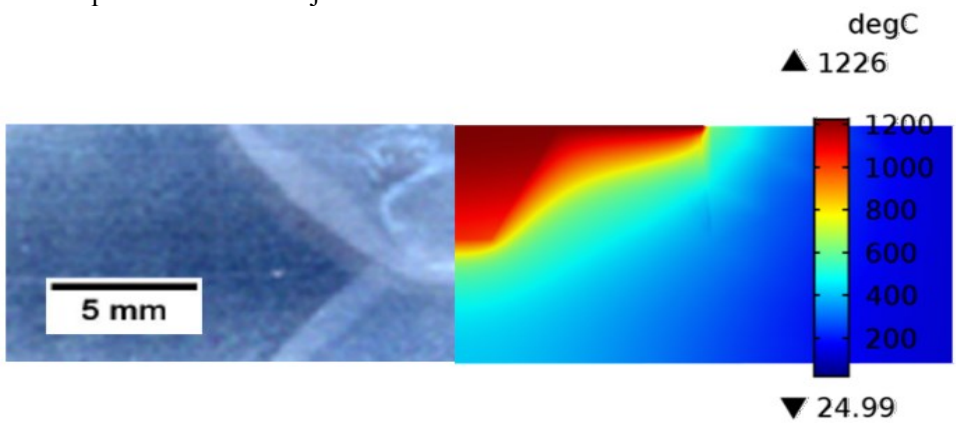


**Fig. 9** Comparative image between the tool and micrography from the welding, considering a hot joint. Adapted from Hermenegildo *et al*. [3]

## CONCLUSION

The current work is an approach to preview temperatures and thermal cycles for different and multivariable welding conditions of API 5L-X80 weld joints of FSW. Considering the difficulty of finding accurate values for the convective coefficients related to the backing plate contact, the thermal model showed a consistent agreement with the experimental values of temperature and with maximum temperatures predicted for the proximities of the welding line. Furthermore, the intrinsic complexity of the FSW experimental setup presented an extra challenge for the feasibility of this model. The simulation helped previewing temperatures in a case where the tool interfered in the temperature acquisition. The model also took minor time to process the computational data, becoming a rapid and straightforward approach to study and understand the thermal phenomena occurring in the FSW of the API 5L-X80.

A correlation with the material's microstructure obtained in previous works can be drawn, once the simulated thermal cycles showed slight differences for maximum temperatures in the tool vicinity. Additionally, the model managed to confirm that peak temperatures in the hot joint were greater than the material's recrystallization temperature, which contributes to martensite formation. This leads to an improved understanding of FSW thermal cycles and its association with the material mechanical properties. It is also pointed out the current work with a mechanical model as the thermocouples located at 12 mm from the welding line have shown divergent values for the maximum temperature.

A coupling model which simultaneously treats complementary contributions of both shearing and frictional, offering a complete computational approach to the FSW processing of API 5L-X80 welds is also in progress.

## ACKNOWLEDGMENTS

The authors would like to acknowledge financial support of Brazilian science agencies CAPES, FACEPE, and CNPq.

## REFERENCES

[1] M. W. THOMAS, E. D. NICHOLAS, J. C. NEEDHAM, M. G. MURCH, P. TEMPLESMITH, C. J. DAWES: 'Friction Stir Butt Welding', *GB Patent Application No. 9125978.8*, December, 1991; US *Patent Application No.* 5460317, October, 1995.

[2] A. SURESH BABU and C. DEVANATHAN: 'An Overview of Friction Stir Welding', *International Journal of research In Mechanical Engineering &Technology*, Vol. 3, No. 2, pp. 259-265, 2013.

[3] T. F. C. HERMENEGILDO, T. F. A. SANTOS, E. A. TORRES, C. R. M. AFONSO, A. J. RAMIREZ: 'Microstructural Evolution of HSLA ISO 3183 X80M (API 5L X80) Friction Stir Welded Joints', *Metals and Materials International,* Vol. 24, No 5, pp. 1120-1132, 2018.

[4] J. A. AVILA, J. RODRIGUEZ, P. R. MEI, A. J. RAMIREZ: 'Microstructure and fracture toughness of multipass friction stir welded joints of API-5L-X80 steel plates', *Materials Science and Engineering: A*, Vol. 673, No. 15, pp. 257-265, 2016.

[5] M. ABBASI, T. W. NELSON and CARL D. SORENSEN: 'Analysis of variant selection in friction-stir-processed high-strength low-alloy steels', *Journal of Applied Crystallography,* Vol. 46, No 3, pp. 716-725, 2013.

[6] M. WITEK: 'Possibilities of Using X80, X100, X120 High-Strength Steels for Onshore Gas Transmission Pipelines', *Journal of natural gas science and engineering*, Vol. 27, Part 1, No. 48, pp. 374–384, 2015.

[7] L. WEI and T. W. NELSON, 'Influence of heat input on post weld microstructure and mechanical properties of friction stir welded HSLA-65 steel', *Materials Science and Engineering: A,* Vol. 556, No. 7, pp. 51-59, 2012.

[8] J. JANOVEC, M. TAKAHASHI, T. KURODA, K. IKEUCHI: 'Microstructural and mechanical aspects of tempered ICCGHAZ of SQV-2A low alloy steel weld', *ISIJ International,* Vol. 40, Suppl. S44-S48, 2000.

[9] AMERICAN PETROLEUM INSTITUTE: '*Welding of Pipelines and Related Facilities, API Standard 1104'* 20th Edition, 2005.

[10] H. SCHIMDT AND J. HATTEL: 'Modelling heat flow around tool probe in friction stir welding', microstructure, and properties", *Science and Technology of Welding and Joining*. Vol. 10, No. 2, pp. 176-186, 2005.

[11] T.W. NELSON, S.A. ROSE, J. MATER: 'Controlling hard zone formation in friction stir processed HSLA steel', *Journal of Materials Processing Technology*, Vol. 231, No. 8, pp. 66–74, 2016.

[12] T. F. A. SANTOS, E. A. TORRES, T. F.C. HERMENEGILDO, A. J. RAMIREZ: 'Development of ceramic backing for friction stir welding and processing' *Welding International*, Vol. *30,* No. 5, pp. 338-347, 2016.

[13] H. CHO; S. HONG; J. ROH; H. CHOI; S. H. KANG; R. J. STEEL; H. N. HAN: 'Three-dimensional numerical and experimental investigation on friction stir welding processes of ferritic stainless steel*', Acta Materialia*, Vol. 61, No. 7, pp. 2649-2661, 2013.

[14] M. SONG, R. KOVACEVIC: 'Thermal modeling of friction stir welding in a moving coordinate system and its validation', *International Journal of Machine Tools and Manufacture*, Vol. 43, No. 6, pp. 605 – 615, 2003.

[15] P. COLEGROVE, M. PAINTER, D. GRAHAM and T. MILLER: '3-dimensional flow and thermal modeling of the friction stir welding process', *The 2nd International Symposium on Friction stir welding*, 2, pp. 1–11, 2000.

[16] Y. J. CHAO, X. QI, W. TANG: 'Heat transfer in friction stir welding experimental and numerical studies', *Journal of Manufacturing Science and Engineering*, Vol.125, No. 1, pp. 138-145, 2003.

[17] M. B. SANTILLANA: 'Thermo-mechanical properties and cracking during solidification of thin slab cast steel', *doctoral thesis*, Technische Universiteit Delft, 2013.

[18] A. SIMAR, J. LECOMTE-BECKERS, T. PARDOEN, B. MEESTER: 'Effect of boundary conditions and heat source distribution on temperature distribution in friction stir welding', *Science and Technology of Welding & Joining,* Vol. 11, No. 2, pp. 170-177, 2006.

[19] M. Z. H. KHANDKAR, J. A. KHAN, A. P. REYNOLDS: 'Prediction of temperature distribution and thermal history during friction stir welding: Input torque-based model', *Science and Technology of Welding & Joining*, Vol. 8, No. 3, pp. 165-174, 2003.

[20] E. J. F. ROCHA, T.S. ANTONINO, P.B. GUIMARAES, R. A. S. FERREIRA, J. M. A. BARBOSA, J. ROHATGI: 'Modeling of the temperature field generated by the deposition of weld bead on a steel butt joint by FEM techniques and thermographic images', *Material Research, São Carlos*, Vol. 21, No. 3, e20160796, 2018.

[21] T. F. A. SANTOS, H. S. IDAGAWA, A. J. RAMIREZ: 'Thermal history in UNS S32205 duplex stainless steel friction stir welds', *Science and Technology of Welding and Joining.* Vol. 19. No. 2. pp. 150-156, 2014.

[22] H. N. B. SCHMIDT and H. J. HATTEL: 'Thermal modelling of friction stir welding', *Scripta Materialia*, Vol. 58, No. 5, pp. 332-337, 2008.

[23] M. MATSUSHITA, Y. KITANI, R. IKEDA, S. ENDO, H. FUJII: 'Microstructure and Toughness of Friction Stir Weld of Thick Structural Steel', *ISIJ International*, Vol. 52, No. 7, pp. 1335–1341, 2012.

[24] R. NANDAN, T. DEBROY, H. K. D. H. BHADESHIA: 'Recent advances in friction-stir welding – process, weldment structure and properties', *Progress in Materials Science*, Vol. 53, No. 6, pp. 980-1023, 2008.

[25] T. F. A. SANTOS, T. F. C. HERMENEGILDO, R. R. MARINHO, M. T. P. PAES, A. J. RAMIREZ: 'Fracture toughness of ISO 3183 X80M (API 5L X80) steel friction stir welds', *Engineering Fracture Mechanics*, Vol. 77, No. 15, pp. 2937-2945, 2010.